PHYSICAL REVIEW E **72**, 026615 (2005)

Homogenization of electromagnetic crystals formed by uniaxial resonant scatterers

Pavel A. Belov
Department of Electronic Engineering, Queen Mary University of London, Mile End Road London, E1 4NS, United Kingdom

Constantin R. Simovski
Photonics and Optoinformatics Department, St. Petersburg State University of Information Technologies, Mechanics and Optics, Sablinskaya 14, 197101, St. Petersburg, Russia

(Received 6 March 2005; published 31 August 2005)

Dispersion properties of electromagnetic crystals formed by small uniaxial resonant scatterers (magnetic or electric) are studied using the local field approach. The goal of the study is to determine the conditions under which the homogenization of such crystals is possible. Therefore the consideration is limited to the frequency region where the wavelength in the host medium is larger than the lattice periods. It is demonstrated that, together with the known restriction for the homogenization related to the large values of the material parameters, there is an additional restriction related to their small absolute values. On the other hand, the homogenization becomes allowed in both cases of large and small material parameters for special directions of propagation. Two unusual effects inherent to the crystals under consideration are revealed: a flat isofrequency contour that allows subwavelength imaging using the canalization regime and birefringence of the extraordinary modes which can be used for beam splitting.

DOI: 10.1103/PhysRevE.72.026615 PACS number(s): 42.70.Qs, 78.20.Ci, 42.25.Gy

I. INTRODUCTION AND PROBLEM FORMULATION

The problem of homogenization of bulk arrays of small scatterers operating in an applied field such as dipoles (electric or magnetic) has a long history. One can recall here the classical works of Lorentz, Madelung, Ewald, and Oseen. However, in what concerns the homogenization of arrays of small resonant scatterers these classical results were revised in the 1970s taking into account the possible shortening of the propagating wave at resonance and the strong mutual coupling of resonant particles. This was done in the seminal work by Sipe and Kranendonk [1]. In the 1990s the interest in this problem was renewed by extensive studies of bianisotropic composites (see, e.g., in [2,3]). Metal bianisotropic particles (chiral particles and omega particles) have small resonant size at microwaves frequencies due to their complex shape (they include a wire ring and straight wire portions). However, the known studies of their homogenization mainly refer to nonregular arrays. This can be explained by the specific applications of microwave bianisotropic composites (as absorbers or antiradar coverings). Work like [4] concerning regular bianisotropic lattices does not consider the effects of particle resonance. Briefly, the homogenization problem for resonant scatterers has not been studied enough. However, it is becoming very important now for the following reasons.

The first one is the rapid development of nanotechnologies. It becomes possible to prepare lattices of metallic nanoparticles operating at frequencies rather close to that of the plasmon resonance of the individual particle. Recently, a significant amount of works has been devoted to one-dimensional (1D) arrays (chains) of silver or gold particles which were found to be good prospects for subwavelength guiding of light (see, e.g., [5] and references therein). It is evident that 2D and 3D lattices of metal nanoparticles provide potentially an even broader scope of optical applications than chains. If the homogenization of a 3D lattice is possible then one can use the basic knowledge of continuous media and apply it to the lattices. This approach can be rather instructive and we demonstrate an example below. In the present paper we study the case of microwave scatterers, but this is only an illustration of the theory. Similar results can be obtained for the optical range, too. Electric scatterers of small resonant size are already known in optics, and the possibility to create small resonant scatterers with magnetic properties was recently shown in [6].

The second motivation of the present research is related to the intensive studies of so-called left-handed media [7]. A left-handed medium (LHM) is an effectively continuous medium with simultaneously negative permittivity and permeability. All-angle negative refraction and backward waves are inherent to such media. The interest in these artificial materials was evoked by the seminal work of Pendry [8] indicating the opportunity of subwavelength imaging using a slab of a LHM. The best-known realization of the LHM is a uniaxial version of this medium studied in [9–11] and others. This structure is composed from two components playing the roles of the building blocks. The first block (responsible for negative permittivity) is a wire medium [12–14] and the second block (responsible for negative permeability) is a lattice of split-ring resonators (SRRs) [15]. The SRRs are small magnetic scatterers experiencing a two-time derivative Lorentz-type resonance. As a result, the permeability of the structure can take negative values within the resonance band of SRRs. This structure operates, however, as a LHM only in the plane orthogonal to the wires (and for only one polarization of the wave). The reason for that is the strong spatial dispersion inherent to wire media at all frequencies [16]. This effect makes the axial component of the wire medium permittivity dependent on the propagation direction. Only for waves propagating in the orthogonal plane this permittivity component is negative for all frequencies below so-called

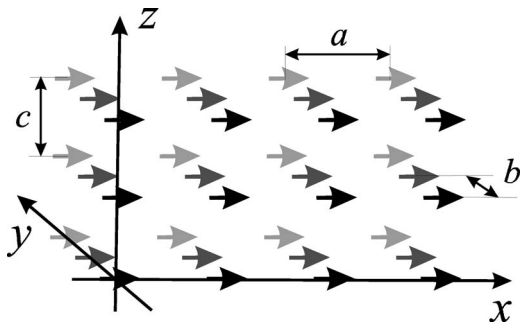

FIG. 1. Geometry of an electromagnetic crystal. The arrows show the directions of the dipole moments of the uniaxial scatterers.

plasma frequency and the structure suggested in [9] can be treated as a LHM only in this special case.

In order to obtain a variant of the LHM operating in three dimensions some attempts to use small resonant electric scatterers together with magnetic ones [17] as well as bianisotropic scatterers [18–20] have been made. The samples of LHMs obtained in [18,20] demonstrate high losses in the LHM regime and this makes the known variants of isotropic LHMs not very interesting.

However, if the goal is to observe negative refraction and backward waves, and to obtain subwavelength images in three dimensions, then the isotropic LHM is not the only solution. These effects can be obtained in anisotropic structures, too, and not only at high frequencies. The so-called indefinite media (in which the principal components of permittivity and permeability tensors have different signs) were studied in [21–23]. These media offer a variety of effects including negative refraction, backward wave effect, near field focusing, high-impedance surface reflection, etc. The anisotropy of the medium introduces additional freedom in manipulation by its dispersion and reflection properties [24]. Even a uniaxial medium with negative permittivity along its axis allows one to observe the effects of negative refraction and backward waves with respect to the interface [25]. The theoretical results [21–23] do not prove that the structure composed of a wire medium and SRRs will demonstrate these effects in practice. On the contrary, from [16,25] it is evident that these effects (which should exist in a continuous uniaxial medium with negative axial permittivity) are absent in wire media. At the same time, a lattice of uniaxial electric scatterers oriented in parallel allows one to obtain the negative axial permittivity for all directions of propagation (i.e., without spatial dispersion). If such a lattice substitutes for the wire medium in the structure reported in [9,10] then the effects predicted in [21–23] for continuous indefinite media can be obtained in practice. This is the second reason for the present study.

In the current paper the dispersion properties of electromagnetic crystals formed by orthorhombic lattices of uniaxial magnetic or electric scatterers are studied. The orientation of scatterers along one of the crystal axes is considered. The geometry of the structure is presented in Fig. 1. As an example of magnetic scatterers we have chosen SRRs [9,10,15] (see Fig. 2). The electric dipoles are represented by short inductively loaded wires (ILWs) [17] (see Fig. 3).

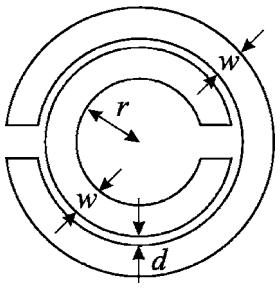

FIG. 2. Geometry of a split-ring-resonator.

An analytical model based on the dipole approximation and the local field approach is introduced. The dipole approximation (magnetic dipoles describing SRRs and electric dipoles describing ILWs) restricts the dimensions of inclusions to be much smaller than the wavelength in the host medium. The local field approach allows us to take into account the dipolar interactions between scatterers exactly. It makes possible accurate studies of lattice resonances. The results allow one to examine when the structure corresponds to a homogenized model of local uniaxial media and when it does not.

It is well known that lattices of resonant scatterers (though they do not exhibit spatial dispersion at all frequencies, unlike wire media) can experience spatial dispersion at low frequencies as compared to the spatial resonance of the lattice. This is the case when the wavelength in the medium becomes comparable with the lattice period [1]. This results in a resonance stopband [1] and the appearance of complex modes within it [19,26]. This makes homogenization impossible within a subband belonging to the resonance band. In the present work we do not pay attention to the complex modes. The comparison of the original lattice and its homogenized model is made using the technique of isofrequency contours. Such an approach allows us to check the correspondence between properties of the structures under consideration and their homogenized models.

A uniaxial medium with negative permittivity (or permeability) along its axis and positive permittivity (or permeability) in the transversal plane has isofrequency contours of hyperbolic form [21–24]. These isofrequencies correspond to negative refraction [22,23]. If both the original lattice and its homogenized model possess such isofrequencies then they both possess negative refraction. More generally, if the homogenized model of the lattice keeps (at least approximately) the same isofrequency contours, then the homogenization is allowed. If the homogenization dramatically changes the contours the homogenization is forbidden. This is the main idea of our approach.

II. MODELS OF INDIVIDUAL SCATTERERS

The geometries of the SRRs and ILW are presented in Figs. 2 and 3, respectively. Since the dipole moments of all

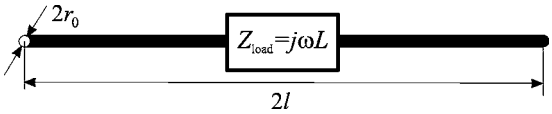

FIG. 3. Geometry of the inductively loaded wire dipole.

scatterers are directed along x (see Fig. 1) an individual scatterer can be characterized by the scalar polarizability α relating the dipole moment to the local field (external field applied to a scatterer).

A. Split-ring resonators

The SRR considered in [9,10,15] is a pair of two coplanar broken rings (see Fig. 2). Since the two loops are not identical the analytical models for such SRRs are rather cumbersome [27,28]. In fact, such a SRR cannot be described as a purely magnetic scatterer, because it exhibits bianisotropic properties and has resonant electric polarizability [27,28] (see also the discussion in [29]). However, the electric polarizability and bianisotropy of SRRs is out of the scope of this paper. We neglect these effects and consider an ordinary SRR as a magnetic scatterer. The analytical expressions for the magnetic polarizability $\alpha(\omega)$ of SRRs with geometry plotted in Fig. 2 were derived and validated in [28]. The final result reads as follows:

$$\alpha(\omega) = \frac{A\omega^2}{\omega_0^2 - \omega^2 + j\omega\Gamma}, \quad A = \frac{\mu_0^2\pi^2 r^4}{L+M}, \tag{1}$$

where ω_0 is the resonant frequency of magnetic polarizability,

$$\omega_0^2 = \frac{1}{(L+M)C_r},$$

L is the inductance of the ring (we assume that both rings have the same inductance),

$$L = \mu_0 r\left[\ln\left(\frac{32R}{w}\right) - 2\right],$$

M is the mutual inductance of the two rings,

$$M = \mu_0 r\left[(1-\xi)\ln\left(\frac{4}{\xi}\right) - 2 + \xi\right], \quad \xi = \frac{w+d}{2r},$$

C_r is the effective capacitance of the SRR,

$$C_r = \varepsilon_0 \frac{r}{\pi}\,\mathrm{arccosh}\left(\frac{2w}{d}\right),$$

Γ is the radiation reaction factor,

$$\Gamma = \frac{A\omega k^3}{6\pi\mu_0},$$

r is the inner radius of the inner ring, w is the width of the rings, d is the distance between the edges of the rings (see Fig. 2), ε_0 and μ_0 are the permittivity and permeability of the host medium, and $k=\omega\sqrt{\varepsilon_0\mu_0}$ is the wave number of the host medium. The presented formulas are valid within the frame of the following approximations: $w,d \ll r$ and the splits of the rings are large enough compared to d. Also, we assume that the SRR is formed of ideally conducting rings (no dissipation losses).

The magnetic polarizability (1) takes into account the radiation losses and satisfies the basic Sipe-Kranendonk condition [1,26,30] which in the present case has the following form:

$$\mathrm{Im}[\alpha^{-1}(\omega)] = \frac{k^3}{6\pi\mu_0}. \tag{2}$$

In the following analysis we operate with the inverse polarizability $\alpha^{-1}(\omega)$; thus, we rewrite Eq. (1) in the form

$$\alpha^{-1}(\omega) = A^{-1}\left(\frac{\omega_0^2}{\omega^2} - 1\right) + j\frac{k^3}{6\pi\mu_0}. \tag{3}$$

B. Inductively loaded short wires

A typical resonant electric scatterer is an inductively loaded short wire, as shown in Fig. 3. The electric polarizability α_e of loaded wires following the known model [17] has the form

$$\alpha_e^{-1} = \frac{3}{l^2 C_{\mathrm{wire}}}\left(\frac{1-\omega^2/\omega_0^2}{4-\omega^2/\omega_0^2}\right) + j\frac{k^3}{6\pi\varepsilon_0} \tag{4}$$

where $C_{\mathrm{wire}} = \pi l\varepsilon_0/\ln(2l/r_0)$ is the capacitance of the wire, $\omega_0 = \sqrt{LC_{\mathrm{wire}}}$ is the resonant frequency, L is the inductance of the load, l is the half length of the wire, and r_0 is the wire radius.

It is clear that at frequencies near the resonance the polarizability of the ILW has the form

$$\alpha_e^{-1}(\omega) \approx A_e^{-1}\left(\frac{\omega_0^2}{\omega^2} - 1\right) + j\frac{k^3}{6\pi\varepsilon_0}, \tag{5}$$

with $A_e = l^2 C_{\mathrm{wire}}$, which is similar to Eq. (3). Moreover, if $A_e/\varepsilon_0 = A/\mu_0$ then using the duality principle the magnetic dipole with polarizability α [Eq. (3)] can be transformed to the electric dipole with polarizability α_e [Eq. (3)], and vice versa. This means that it is enough to consider only one type of resonant scatterer. In the present paper we have chosen magnetic ones to be principal. The electric scatterers can be easily obtained using the duality principle from the magnetic scatterers by $A = \mu_0 A_e/\varepsilon_0$.

III. HOMOGENEOUS MEDIA APPROACH

Let us consider an orthorhombic lattice with periods $a \times b \times c$ formed by magnetic uniaxial scatterers directed along x (see Fig. 1) and described by the polarizability (1). For electric scatterers (ILWs) the problem is dual to the present one. In the long wavelength limit the lattices of scatterers are usually described as homogeneous media with certain material parameters. The lattice under study can be modeled as a resonant uniaxial magnet. The permeability of such a magnet is a dyadic of the form

$$\bar{\bar{\mu}} = \mu \mathbf{x}_0\mathbf{x}_0 + \mu_0(\mathbf{y}_0\mathbf{y}_0 + \mathbf{z}_0\mathbf{z}_0).$$

The permeability μ (x component of the tensor) can be calculated though the individual polarizability of a single scatterer using the Clausius-Mossotti formula [31]

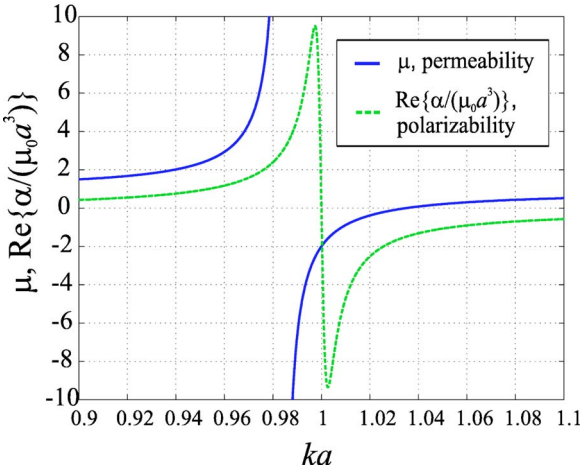

FIG. 4. (Color online) Dependencies of relative permeability μ/μ_0 and normalized polarizability $\alpha/(\mu_0 a^3)$ vs normalized frequency ka for cubic lattice ($a=b=c$) of SRRs with $A=0.1\mu_0 a^3$ and $\omega_0=1/(a\sqrt{\varepsilon_0\mu_0})$.

$$\mu = \mu_0\left(1 + \frac{\alpha(\omega)/(\mu_0 V)}{1 - C_s(a,b,c)\alpha(\omega)/\mu_0}\right), \tag{6}$$

where $V=abc$ is the volume of the lattice elementary cell and $C_s(a,b,c)$ is the static interaction constant of the lattice. The following expression for this interaction constant is available in (Ref. [31], p. 758):

$$\begin{aligned} C_s(a,b,c) &= \frac{1}{4\pi}\sum_{(m,n,l)\neq(0,0,0)} \frac{2(am)^2-(bn)^2-(cl)^2}{[(am)^2+(bn)^2+(cl)^2]^{5/2}} \\ &= \frac{1.202}{\pi a^3} - \frac{4\pi}{a^3}\sum_{(n,l)\neq(0,0)}\sum_{m=1}^{+\infty} m^2 \\ &\quad \times K_0\left(\frac{2\pi m}{a}\sqrt{(bn)^2+(cl)^2}\right), \end{aligned} \tag{7}$$

where $K_0(x)$ is the modified Bessel function of the third kind (the McDonald function). In the case of a cubical lattice $a=b=c$ the interaction constant is equal to the classical value $C_s=1/(3V)$.

Notice that the radiation loss contribution in expression (3) should be skipped when substituting into formula (6). This makes permeability a purely real number as it should be for lossless regular arrays [1,26]. This manipulation is based on the fact that the far-field radiation of the single scatterer is compensated by the electromagnetic interaction in a regular three-dimensional array, so that there is no radiation loss for the wave propagating in the lattice. The mathematical proof of this fact for general dimensions of the lattice is presented in the Appendix.

The typical dependence of the magnetic permeability μ on frequency is presented in Fig. 4 for a cubic lattice ($a=b=c$) of SRRs with parameters chosen so that $A=0.1\mu_0 a^3$ and $\omega_0=1/(a\sqrt{\varepsilon_0\mu_0})$. The resonant frequency shift from $ka=1$ to 0.984 is clearly observed. While $ka<0.984$ the structure is paramagnetic ($\mu>1$). For ka within the [0.984, 1.0352] range the permeability is negative ($\mu<0$). For $ka>1.0352$ the medium is diamagnetic ($0<\mu<1$).

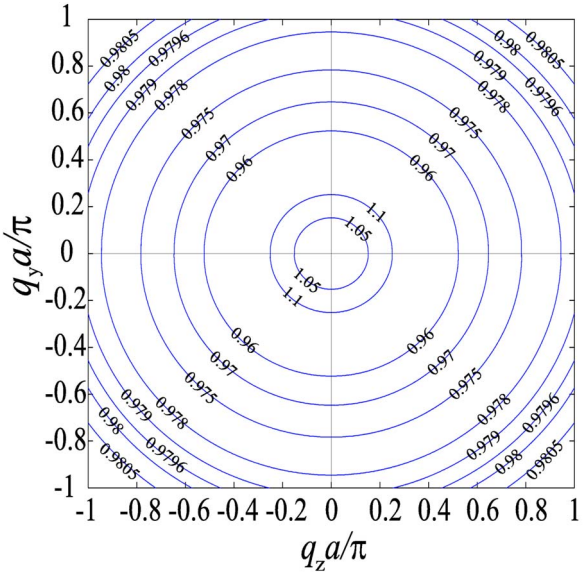

FIG. 5. (Color online) Isofrequency contours in the yz plane for a uniaxial magnetic material with permeability as in Fig. 4. The numbers correspond to values of ka.

The dispersion equation for the uniaxial magnetic medium has the following form (see, e.g., [24,25,31]):

$$\mu_0(q_y^2+q_z^2) = \mu(k^2-q_x^2). \tag{8}$$

Thus, the isofrequency surfaces for such materials have the form of a spheroid if $\mu>0$ (the spheroid is prolate for $\mu<1$ and oblate for $\mu>1$) or a hyperboloid if $\mu<0$. Both types of isofrequency surface have the symmetry axis along x.

The medium is isotropic in the yz plane (the isofrequency contours in this plane are circles; see Fig. 5). Thus, we can restrict our consideration to the xy plane without loss of generality. The typical isofrequency contours in this plane are shown in Figs. 6 and 7. The magnetic under consideration has the same parameters as in Fig. 4. The ranges of wave vector components q_x and q_y are restricted to $\pm\pi/a$ and $\pm\pi/b$, respectively, having in mind that the exact dispersion diagram of the lattice corresponds to the first Brillouin zone, and we will compare the homogenized model with the exact theory.

While the frequency is below the resonance ($ka<0.984$) the isofrequency contour has the form of an ellipse prolate along the y axis ($\mu>1$). For frequencies above the resonance but less than the frequency at which the permeability turns to zero ($0.984<ka<1.0352$) the isofrequency contours are hyperbolas ($\mu<0$) (see Fig. 4). If the frequency is above the frequency at which the permeability passes zero ($ka>1.0352$) then the isofrequency contour becomes an ellipse oblate along the y axis ($0<\mu<1$). All the isofrequency contours pass through the points $q_x=\pm k$. In particular, all the ellipses have the same semiaxes along x (equal to k). Notice

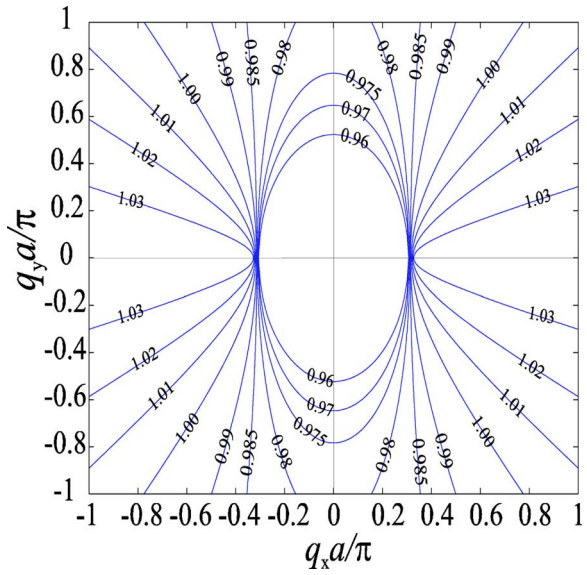

FIG. 6. (Color online) Isofrequency contours in the xy plane for uniaxial magnetic material with permeability as in Fig. 4 for frequencies near the resonance of the permeability. The numbers correspond to values of ka.

that the solution $q_x=k$ corresponds also to arbitrary values of q_y, q_z if $\mu \to \infty$. This implies the propagation of all waves along the optical axis x with the same phase velocity which is equal to that of the host medium. Strictly speaking, for an infinite value as well as for finite large values of μ the homogenization is forbidden. But we will show using the local field method that the homogenization is allowed even at a frequency such that $\mu \to \infty$ if one restricts consideration to a special case of propagation. In general, it turns out that at all frequencies there are special cases of propagation for which the homogenization is allowed.

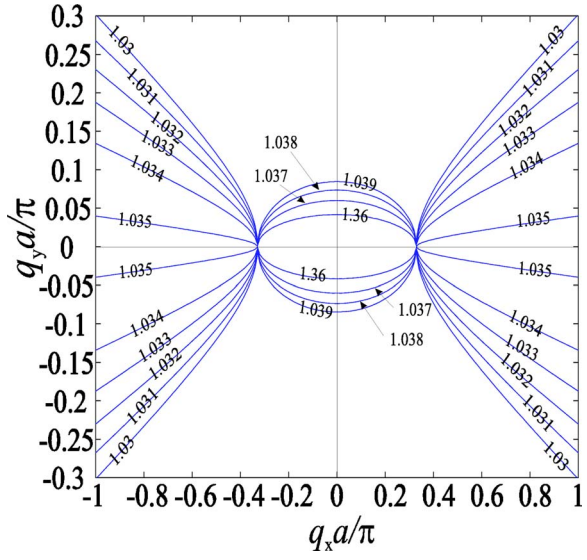

FIG. 7. (Color online) Isofrequency contours in the xy plane for uniaxial magnetic material with permeability as in Fig. 4 for the frequencies where the permeability is close to zero. The numbers correspond to values of ka.

The hyperbolic form of the isofrequency contour is a unique feature inherent to resonant uniaxial magnets [21–25]. It allows one to achieve negative refraction at all incident angles for p polarization if the interface is normal to the optical axis. In the case of a resonant uniaxial dielectric medium the same effect happens for s polarization. If the uniaxial medium is two component and has both negative axial permittivity and permeability, the negative refraction should be observed for both p and s polarizations [21–25].

Below we will compare Figs. 6 and 7 with those calculated for an original lattice of SRRs using the exact approach.

IV. DISPERSION EQUATION FOR ELECTROMAGNETIC CRYSTALS FORMED BY UNIAXIAL SCATTERERS

Following the local field approach the dipole moment M of a zero-numbered scatterer is determined by the magnetic field $\mathbf{H}_{\text{loc}}$ acting on this scatterer: $M=\alpha H^x_{\text{loc}}$, where $H^x_{\text{loc}}=(\mathbf{H}_{\text{loc}}\cdot\mathbf{x}_0)$. This local field is the sum of the magnetic fields $\mathbf{H}_{m,n,l}$ produced at the coordinate origin by all other scatterers with indices $(m,n,l)\neq(0,0,0)$:

$$\mathbf{H}_{\text{loc}}=\sum_{(m,n,l)\neq(0,0,0)}\mathbf{H}_{m,n,l}. \tag{9}$$

The magnetic field produced by a single scatterer with index (m,n,l) is given by the dyadic Green's function $\bar{\bar{G}}(\mathbf{R})$:

$$\mathbf{H}_{m,n,l}=\mu_0^{-1}\bar{\bar{G}}(\mathbf{R}_{m,n,l})\mathbf{M}_{m,n,l}, \tag{10}$$

where

$$\bar{\bar{G}}(\mathbf{R})=(k^2\bar{\bar{I}}+\boldsymbol{\nabla}\boldsymbol{\nabla})\frac{e^{-jkR}}{4\pi R}.$$

We consider uniaxial scatterers oriented along the $\mathbf{x}_0$ direction, so it is enough to use only the $\mathbf{x}_0\mathbf{x}_0$ component of the dyadic Green's function. So we replace Eq. (10) by the scalar expression

$$H^x_{m,n,l}=\mu_0^{-1}G(\mathbf{R}_{m,n,l})M_{m,n,l}, \tag{11}$$

where

$$G(\mathbf{R})=\left(k^2+\frac{\partial^2}{\partial x^2}\right)\frac{e^{-jkR}}{4\pi R}$$
$$=\left[(1+jkR)\frac{2x^2-y^2-z^2}{R^4}+k^2\frac{y^2+z^2}{R^2}\right]\frac{e^{-jkR}}{4\pi R}.$$

To study eigenmodes of the system we introduce the phase distribution of dipole moments determined by the unknown wave vector $\mathbf{q}=(q_x,q_y,q_z)^T$ as follows:

$$M_{m,n,l}=Me^{-j(q_xam+q_ybn+q_zcl)}. \tag{12}$$

Collecting together expressions (9), (11), and (12) we obtain a dispersion equation relating the wave vector $\mathbf{q}$ to the frequency ω:

$$M=\alpha\mu_0^{-1}\sum_{(m,n,l)\neq(0,0,0)}G(\mathbf{R}_{m,n,l})Me^{-j(q_xam+q_ybn+q_zcl)}.$$

It can be rewritten in a more appropriate form as

$$[\mu_0\alpha^{-1}(\omega) - C(k,\mathbf{q})]M = 0, \tag{13}$$

where

$$C(k,\mathbf{q},a,b,c) = \sum_{(m,n,l)\neq(0,0,0)} G(\mathbf{R}_{m,n,l})e^{-j(q_x am+q_y bn+q_z cl)}. \tag{14}$$

We call C the dynamic interaction constant of the lattice using the analogy with the classical interaction constant from the theory of artificial dielectric and magnetics materials [31].

The dispersion equation (13) has two different types of solution. The first ones are ordinary waves with zero dipole moments ($M=0$). They are plane waves propagating in the host medium which have zero component of magnetic field along the direction of the dipoles. They do not interact with the lattice (do not excite magnetodipole moments). The waves of the second type are extraordinary waves. They excite magnetodipole moments ($M\neq 0$) strongly interacting with each other. The dispersion equation for extraordinary modes transforms Eq. (13) to

$$\mu_0\alpha^{-1}(\omega) - C(k,\mathbf{q},a,b,c) = 0. \tag{15}$$

The solution of this dispersion equation allows us to study dispersion diagrams for the crystal under consideration. The main problem is the calculation of the dynamic interaction constant C given by Eq. (14). This question is closely related to such concepts as the static interaction constant (7) and the triply periodic dyadic Green's function. The static interaction constant can be obtained from Eq. (14) by letting $k=q_x=q_y=q_z=0$ and choosing the appropriate order of summation for the conditionally convergent series obtained [32]. The planewise summation method [32,33] or Poisson summation formula based technique [31,34] is usually applied for calculation of the static interaction constant. The triply periodic dyadic Green's function represents the field produced by a phased lattice of point dipoles. If the zero-numbered term is added to the series (14) [simultaneously one should move the observation point in Eq. (10) from the node of the lattice to avoid singularity] the formula (14) will give a copolarized component of the dyadic Green's function. The triply periodic dyadic Green's function is usually evaluated with the help of the classical Ewald method [35–37]. However, other methods of summation (with improved convergence rate) exist as well [38,39]. All the methods listed above can be applied for evaluation of the dynamic interaction constant (14). The Ewald method requires appropriate choice of splitting parameter [40], which is a sophisticated manipulation. Also, it does not show the energy balance in the lattice (neither do the other methods mentioned above). Therefore, we have chosen a different method of summation. Our approach combines the planewise summation [32,33] and the Poisson summation technique with singularity cancellation [31]. Details of the evaluation of C, which includes the energy balance condition as an intermediate step, are presented in the Appendix.

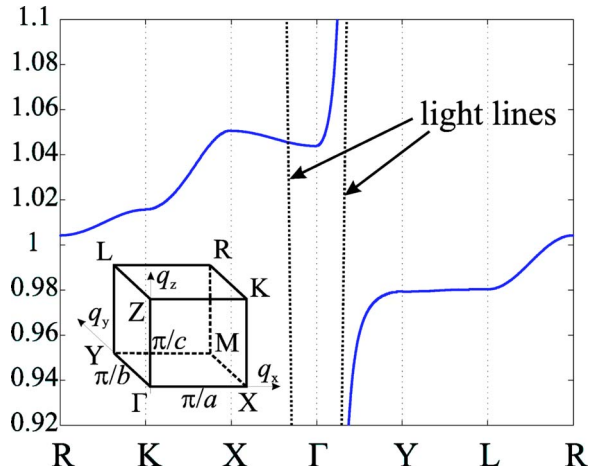

FIG. 8. (Color online) Dispersion diagram for cubic lattice ($a=b=c$) of SRRs with $A=0.1\mu_0 a^3$ and $\omega_0=1/(a\sqrt{\varepsilon_0\mu_0})$.

V. DISPERSION PROPERTIES OF THE CRYSTAL

The dispersion equation (15) with interaction constant $C(k,\mathbf{q})$ given by formula (A37) from the Appendix is solved numerically. The parameters of the structure are the same as those of the homogenized structure: cubic lattice ($a=b=c$) of SRRs, $A=0.1\mu_0 a^3$, and $\omega_0=1/(a\sqrt{\varepsilon_0\mu_0})$. The dispersion diagram for the crystal is presented in Fig. 8. The points $\Gamma=(0,0,0)^T$, $X=(\pi/a,0,0)^T$, $Y=(0,\pi/a,0)^T$, $L=(0,\pi/a,\pi/a)^T$, $K=(\pi/a,0,\pi/a)^T$, and $R=(\pi/a,\pi/a,\pi/a)^T$ of the first Brillouin zone are illustrated in the sketch in the left bottom corner of the plot. The dotted lines represent dispersion curves for ordinary modes of the crystal which coincide with light lines. An incomplete resonant stopband for extraordinary modes (similar to those discussed in [26]) is observed in the vicinity of the resonance of individual inclusions.

The dispersion curve for the (010) direction (branch ΓY in Fig. 8) is shown in Fig. 9 for comparison with result predicted by homogenization model. For this direction of propa-

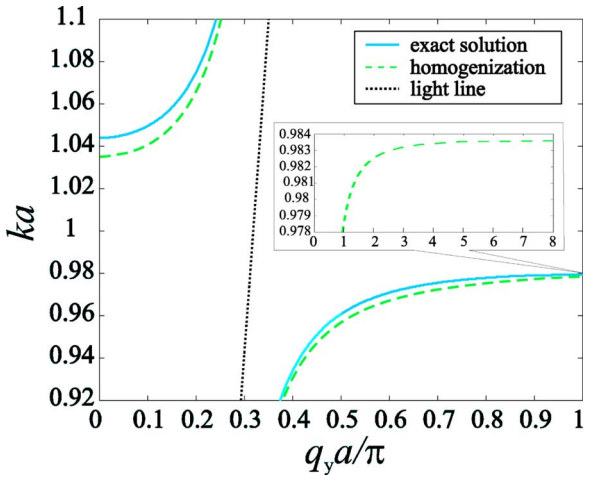

FIG. 9. (Color online) Dispersion curve for (010) direction. Exact solution (solid line), prediction by homogenization model (dashed line), and light line (dotted line).

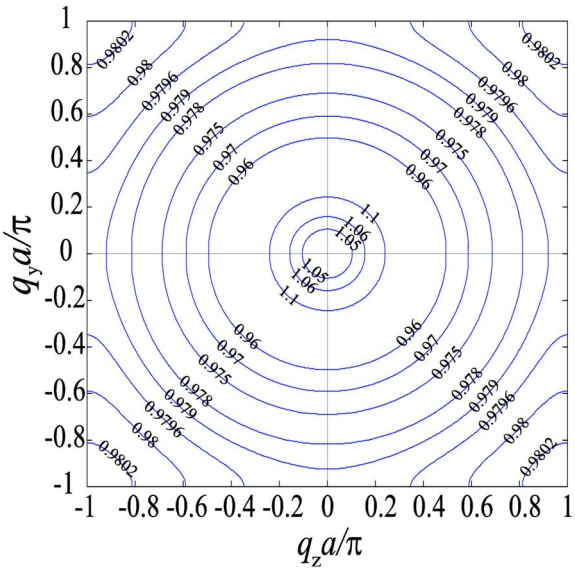

FIG. 10. (Color online) Isofrequency contours in the yz plane for frequencies near the top and bottom edges of the stopband. The numbers correspond to values of ka.

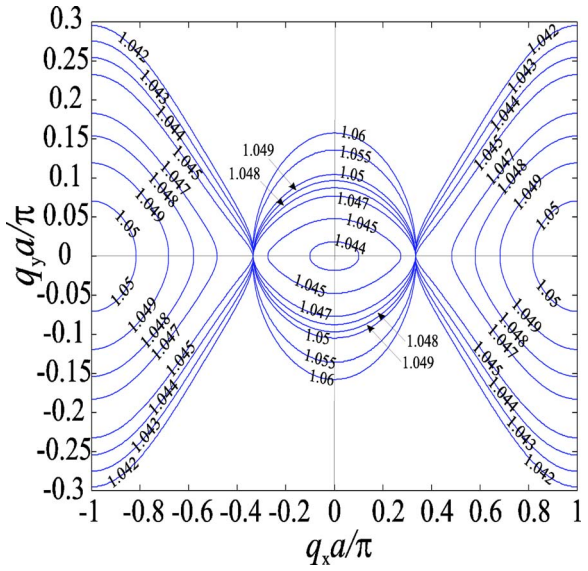

FIG. 11. (Color online) Isofrequency contours in the xy plane for frequencies near the top edge of the stop band. The numbers correspond to values of ka.

gation the agreement with the homogenized model is fine except in the narrow frequency range $0.979 < ka < 0.984$. This region is shown in the inset of Fig. 9 and it is clear from Fig. 8 that it corresponds to the lower edge of the stopband for waves propagating in the transverse plane (yz). This frequency range in the homogenization model corresponds to a high propagation constant $q_y > \pi/a$ and a high positive permeability $\mu > \pi^2/(ka)^2$. This means that the homogenization in the case $\mu > \pi^2/(ka)^2$, strictly speaking, describes the dispersion of the lattice in a wrong manner. This is an expected result which corresponds to the known predictions of the classical theory [1]. Below we will consider this frequency range in detail.

The frequency band $0.9803 < ka < 1.044$ corresponds to negative axial permittivity of the homogenized model of the lattice. Negative axial permittivity means an imaginary propagation constant for the transverse plane and this result nicely corresponds to the stop band for the yz plane predicted by the exact theory. So homogenization within $0.9803 < ka < 1.044$ is allowed.

The isofrequency contours in the yz plane for frequencies near the bottom $0.96 < ka < 0.9803$ and top $1.04 < ka < 1.10$ edges of the transverse stop band are presented in Fig. 10. The behavior of isofrequency contours shown in Fig. 10 is typical for general electromagnetic crystals at frequencies near the stop band edges [41–43]. While the frequency is rather far below the stop band ($ka < 0.979$) the isofrequency contours have the form of circles and the agreement with the homogenized model is fine (see Fig. 5). The same behavior is observed above the stop band ($ka > 1.044$). The circles for $ka > 1.044$ are smaller than those for $ka < 0.979$ which nicely corresponds to the smaller effective permeability (see Fig. 4). However, within the narrow frequency range $0.979 < ka < 0.9803$ the isofrequency contours acquire a form that is different from a circle. This anisotropy in the transverse plane gives evidence of spatial dispersion. Notice that in this band in the lattice there are two evanescent modes whose wave vectors lie in the transverse plane (see also [26]). Strictly speaking, the crystal cannot be homogenized at these frequencies, and these frequencies correspond to a high positive μ of the homogenized lattice. It was already noticed above that this is the expected result.

Significant disagreement between the exact solution and the result of homogenization was also obtained at frequencies near the top edge of the stop band. The isofrequency contours in the xy plane for this frequency range are presented in Fig. 11. They dramatically differ from the prediction given by the homogenization model shown in Fig. 7. Following the homogenization approach, the isofrequency contours should have a hyperbolic form at frequencies corresponding to a negative effective permittivity and an elliptic one in the case of positive permittivity (see Fig. 7). The exact modeling reveals that this switching between hyperbolic and elliptic types of isofreqency contours happens in a different manner. When $ka < 1.0435$ the isofrequency contours have a form that is similar to a hyperbolic one but they are already distorted. At the higher frequencies $ka > 1.0435$ the "hyperbolic" contours continue to distort, and simultaneously "elliptic" contours (the second branch of the same isofrequency) appear in vicinity of the Γ point. The hyperbolic contours pass through points $q_x = \pm k$ while $ka < 1.0455$, but elliptic ones do not. For $ka > 1.046$ the situation changes to the opposite one. The elliptic contours acquire a fixed size along the x axis and start to pass through points $q_x = \pm k$. On the other hand, the hyperbolic contours start to collapse around the X point and completely disappear for $ka > 1.051$. In this way the hyperbolic contours transform to elliptic ones passing through the regime where both types of contours coexist at the same frequencies. At any frequency only one of these contours passes through the points $q_x = \pm k$.

Thus, in the region $1.043 < ka < 1.051$ homogenization gives the wrong results for the waves propagating in the xy

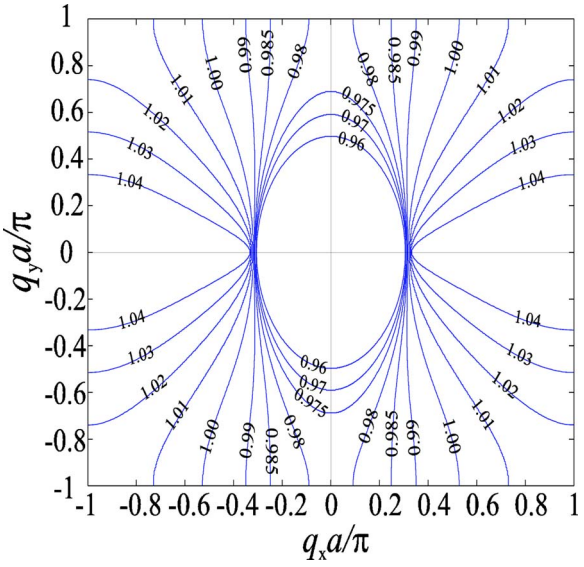

FIG. 12. (Color online) Isofrequency contours in the xy plane for frequencies near the bottom edge of the stop band. The numbers correspond to values of ka.

plane because of the two-mode regime observed in the original structure. This region corresponds to small absolute values of μ ($|\mu|<0.2$ in our case). Strictly speaking, homogenization in the region of small $|\mu|$ turns out to be forbidden. In our opinion, this is a qualitatively new result. However, as follows from Fig. 10 the homogenized model makes the correct prediction for waves propagating in the yz plane in the band $1.043<ka<1.051$. One can conclude that homogenization at these frequencies (forbidden in its strict meaning) is allowed for the case of transversal propagation.

The described regime of the coexistence of hyperbolic and elliptic isofrequency contours at a fixed frequency means birefringence for extraordinary modes and three-refringence in the case of refraction (one ordinary wave and two extraordinary ones). The extraordinary mode corresponding to the hyperbolic contour refracts negatively, and the other one (corresponding to the elliptic contour) experiences positive refraction. This property can find different applications (beam splitting, etc.).

VI. CANALIZATION REGIME AND SUBWAVELENGTH IMAGING

Above, we pointed out that near the bottom edge of the stop band (frequencies corresponding to high positive μ) the homogenized model wrongly predicts the dispersion of waves propagating in the yz plane. Now let us show that the homogenized model gives the qualitatively correct predictions in this frequency region if consideration is restricted to propagation in the xy plane. The isofrequency contours in the xy plane for frequencies near the bottom edge of the stop band are presented in Fig. 12. The behavior of the contours is in the good agreement with the predictions of the homogenized model (see Fig. 6). A difference is noticed only near the edges of the lowest Brillouin zone. So homogenization (forbidden in its strict meaning for $ka\approx0.98$) is still allowed for the case of oblique propagation with respect to the optical axis.

At frequencies near $ka=0.989$ the isofrequency contours are practically flat. This means that all eigenmodes at such frequencies have the same axial component $q_x=\pm k$ of the wave vector. Moreover, they all have the same group velocity (the group velocity is normal to the isofrequency contour). This causes the eigenmode to be the so-called transmission line mode, like that of a wire medium [16]. For both a lattice of uniaxial scatterers and a wire medium this isofrequency corresponds to the infinite material parameter of the homogenized model. The difference is that in the present case the flat isofrequency contour exists at a single frequency $ka=0.989$, in contrast to the wire medium, which supports transmission line modes in a very wide frequency range.

Note that the presence of flat isofrequency contours is not a specific feature of the crystals studied here. The flat isofrequency contours can be found in the band structures of various periodic media, especially close to the band gap edges, as exemplified in photonic crystals or in electronic bands of semiconductors.

The flat isofrequency contours we have found can be used for the implementation of the so-called canalization regime described in our recent paper [43]. Similar regimes are called also self-guiding [44], directed diffraction [45], self-collimation [46], and tunneling [47]. In [43] we have shown that not only all propagating spatial harmonics will be transformed into a strictly parallel beam at the frequency corresponding to the flat isofrequency contour; all evanescent waves impinging on the medium at this frequency will also be transformed into a plane wave with $q_x=k$ transporting the energy along the optical axis. Therefore this regime allows creation of subwavelength images of the sources and transmission of their near field to unrestricted distances.

The canalization regime for a slab of medium possessing a flat isofrequency does not involve negative refraction and amplification of evanescent modes, which are usually used for that purpose [8,42,48]. Its main feature is transformation of the spatial spectrum of the incident field into a collimated beam directed across the slab. All spatial harmonics of the source refract into such eigenmodes at the front interface. These eigenmodes all propagate normal to the interface with the same velocity and deliver the input distribution of the electric field to the back interface. Their refraction at the back interface forms the image. The problem of reflection from a slab (and inner reflections in the slab) can be solved using Fabry-Pérot resonance. The Fabry-Pérot resonance holds for all incidence angles including complex angles. The reason for that is simple: after the refraction all the incident waves acquire the same longitudinal component of the wave vector $q_x=k$. Thus, in the canalization regime there is no image deterioration because of the finite thickness of the lens (there are no waves traveling along the interfaces).

VII. CONCLUSION

In the present paper we have studied dispersion properties of electromagnetic crystals formed by uniaxial resonant scatterers (magnetic and electric ones). The structures are mod-

eled using the local field approach. The main tricky point of this theory is evaluating the dynamic interaction constant of the lattice. This constant has been calculated using a special analytical method based on a planewise summation approach, the Poisson summation formula, the singularity cancellation technique, and the convergence acceleration of slowly convergent series. As a result, a transcendental dispersion equation has been obtained in a form suitable for rapid and efficient numerical calculations. Comparison of the exact solution provided by this equation with the homogenization model allows us to show that the structure, strictly speaking, cannot be homogenized not only at frequencies that correspond to very high values of the effective permeability or permittivity (this was well known earlier) but also at frequencies corresponding to small absolute values of them.

However, if one is interested in special cases of propagation then homogenization can be allowed in both these frequency bands. For propagation in the plane comprising the optical axis, homogenization is allowed in the region of large material parameters. For propagation in the plane orthogonal to the optical axis, homogenization is allowed in the region of small material parameters.

It has been already known since the 1970s [1] that the method of local fields stresses the difference between the homogenized model and the theory of a discrete lattice of scatterers. This is because this method considers the scatterers as point dipoles whose reradiated field is singular at their centers. Actually, the true field is spread over the domain of real scatterers, and the homogenized model should work better than the method of local fields predicts. The discrepancy between the effective medium model and the model of the discrete lattice that we have shown in the present work is in this meaning the maximal one. The results we have presented refer to a simple cubic lattice, though the corresponding analysis can be easily made for orthorhombic lattices, and the bounds of the homogenized model outlined above are basically the same.

Unfortunately, in experimental work dealing with lattices of resonant uniaxial scatterers, like [49], the authors usually consider only the special case of propagation: namely, propagation in the plane orthogonal to the optical axis of the crystal. If the authors of these reports considered propagation along the optical axis or even obliquely with respect to it, then they could see that at certain frequencies the homogeneous medium approach does not work.

During our study we have also found two interesting properties of the crystals under consideration. At a single frequency near the bottom edge of the stop band the isofrequency contour is flat and this frequency corresponds to infinite permeability or permittivity. This fact makes it possible to use the crystals for subwavelength imaging. The two-mode regime is observed at frequencies near the top edge of the stop band. This corresponds to birefringence for extraordinary waves and to three-refringence of the incident wave in the general case of arbitrary polarization, which can be used for beam splitting.

The dispersion theory presented in this paper is a powerful tool for dispersion analysis of three-dimensional electromagnetic crystals. In the present form the theory is restricted to the case of simple (uniaxial) scatterers, but it can be extended to the case of electric or magnetic scatterers with an arbitrary dyadic response. This will be done in our future publications. In this case it will be possible to develop an analytical theory for a lattice of isotropic resonant scatterers (e.g., metallic spheres in the optical range) in a more accurate manner than the known low-frequency approximations [31,34,35,50] allow one to do. This can be useful for the field of optics of metal nanoparticles, which is developing fast.

APPENDIX: EVALUATION OF DYNAMIC INTERACTION CONSTANT

For calculation of the dynamic interaction constant $C(k,\mathbf{q})$ [Eq. (14)] we apply a method based on planewise summation, Poisson summation formulas, and the singularity cancellation technique. This method was applied in [51] for calculation of the two-dimensional dynamic interaction constant for the theory of doubly periodic wire lattices. The series in Eq. (14) are divergent in the classical meaning, but the physical reasoning for the necessary type of summation is clear enough. Due to the existence of losses in real space one should add an infinitesimal imaginary part to the wave vector k of free space and tend it to zero in order to get the correct result.

We split the series (14) (remember that the zero term is excluded from the summation) into three parts:

$$\sum_{l\neq 0}\sum_{m=-\infty}^{+\infty}\sum_{n=-\infty}^{+\infty} + \sum_{n\neq 0}\sum_{m=-\infty}^{+\infty}\Bigg|_{l=0} + \sum_{m\neq 0}\Bigg|_{l=n=0}.$$

These parts are denoted as $C_{1,2,3}$ respectively, and $C=C_1+C_2+C_3$. The splitting areas are shown in Fig. 13. The term C_1 describes the contribution to the local field from all plane grids that are parallel to the xy plane except the grid located in this plane. The term C_2 corresponds to the contribution of the dipole linear chains parallel to the x axis and located in the xy plane except the chain located on this axis. The term C_3 is the contribution from all dipoles of the chain located on the x axis except the dipole located at the origin of the coordinate system. Notice that C_2+C_3 gives the interaction constant of the planar grid.

For evaluation of the term C_1 it is possible to use the Poisson summation formula for double series which leads to an expression with rapidly (exponentially) convergent series. The term C_2 can be calculated using the ordinary Poisson summation formula together with the singularity cancellation technique [31]. It is impossible to apply the Poisson summa-

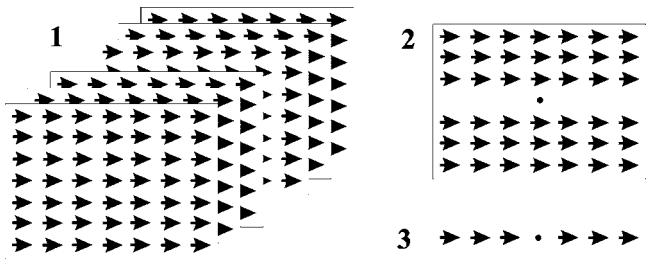

FIG. 13. Splitting areas.

tion formula for evaluation of the term C_3 since it contains a noncomplete series. Convergence of these series can be accelerated using dominant part extraction [52].

1. Contribution of parallel planar grids

The double Fourier transformation of any function $f(x,y)$ is defined as follows:

$$F(p,q) = \mathbf{L}_{x,y}\{f(x,y)\} = \int_{-\infty}^{+\infty}\int_{-\infty}^{+\infty} f(x,y)e^{-j(px+qy)}dx\,dy.$$

The Poisson summation formula for double series has the following form [31]:

$$\sum_{m=-\infty}^{+\infty}\sum_{n=-\infty}^{+\infty} f(am,bn) = \frac{1}{ab}\sum_{m=-\infty}^{+\infty}\sum_{n=-\infty}^{+\infty} F\left(\frac{2\pi m}{a},\frac{2\pi n}{b}\right). \tag{A1}$$

The double Fourier transform of the Hertz potential of a dipole reads

$$\mathbf{L}_{x,y}\left\{\frac{1}{4\pi}\frac{e^{-jk\sqrt{x^2+y^2+z^2}}}{\sqrt{x^2+y^2+z^2}}\right\} = \frac{1}{2}\frac{e^{-|z|\sqrt{p^2+q^2-k^2}}}{\sqrt{p^2+q^2-k^2}}, \tag{A2}$$

where the sign of the square root should be chosen so that $\mathrm{Im}(\sqrt{p^2+q^2-k^2}) \geqslant 0$.

Applying the shift and differential properties of the Fourier transformation to the Fourier image of the Hertz potential (A2) we obtain the transformation rule

$$\mathbf{L}_{x,y}\left\{\left[\left(k^2+\frac{\partial^2}{\partial^2 x}\right)\frac{e^{-jk\sqrt{x^2+y^2+z^2}}}{\sqrt{x^2+y^2+z^2}}\right]\frac{e^{-j(q_x x+q_y y)}}{4\pi}\right\}$$
$$= \frac{k^2-(q_x+p)^2}{2}\frac{e^{-|z|\sqrt{(q_x+p)^2+(q_y+q)^2-k^2}}}{\sqrt{(q_x+p)^2+(q_y+q)^2-k^2}}. \tag{A3}$$

Using the Poisson summation formula (A1) together with (A3) we obtain the term C_1 in the form

$$C_1 = \sum_{l\neq 0}\sum_{m=-\infty}^{+\infty}\sum_{n=-\infty}^{+\infty}\frac{jp_m^2}{2ab}\frac{e^{-j(|cl|k_z^{(mn)}+q_z cl)}}{k_z^{(mn)}}, \tag{A4}$$

where

$$k_x^{(m)} = q_x + \frac{2\pi m}{a}, \quad k_y^{(n)} = q_y + \frac{2\pi n}{b},$$

$$p_m = \sqrt{(k_x^{(m)})^2 - k^2},$$

$$k_z^{(mn)} = -j\sqrt{(k_x^{(m)})^2 + (k_y^{(n)})^2 - k^2}.$$

Here we choose $\mathrm{Im}(\sqrt{\cdot}) \geqslant 0$, so that $\mathrm{Im}(k_z^{(mn)}) \leqslant 0$. The representation (A4) can be treated as an expansion of the fields produced by parallel dipole grids in terms of the Floquet modes. The wave vectors of these modes are

$$\mathbf{k}^{(mn)} = (k_x^{(m)}, k_y^{(n)}, k_z^{(mn)})^T.$$

The series with index l in Eq. (A4) are geometrical progressions and their summation can be made directly:

$$\sum_{l\neq 0} e^{-j(|cl|k_z^{(mn)}+q_z cl)} = -\frac{e^{-jk_z^{(mn)}c} - \cos q_z c}{\cos k_z^{(mn)}c - \cos q_z c}.$$

This allows one to rewrite expression (A4) for the term C_1 as

$$C_1 = \sum_{m=-\infty}^{+\infty}\sum_{n=-\infty}^{+\infty}\frac{p_m^2}{2jabk_z^{(mn)}}\frac{e^{-jk_z^{(mn)}c} - \cos q_z c}{\cos k_z^{(mn)}c - \cos q_z c}. \tag{A5}$$

These series possess exponential convergence. It is clearly seen if the second factor of the term under the summation in Eq. (A5) is rewritten as

$$-\left[\frac{1}{e^{j(k_z^{(mn)}+q_z)cl}-1} + \frac{1}{e^{j(k_z^{(mn)}-q_z)cl}-1}\right].$$

This makes Eq. (A5) suitable for rapid numerical calculations.

2. Contribution of parallel chains from *xy* plane

The ordinary Fourrier transformation has the form

$$F(p) = \mathbf{L}_x\{f(x)\} = \int_{-\infty}^{+\infty} f(x)e^{-jpx}dx.$$

Poisson's summation formula for single series reads

$$\sum_{m=-\infty}^{+\infty} f(am) = \frac{1}{a}\sum_{m=-\infty}^{+\infty} F\left(\frac{2\pi m}{a}\right). \tag{A6}$$

The Fourier transform for the Hertz potential of a dipole is

$$\mathbf{L}_x\left\{\frac{1}{4\pi}\frac{e^{-jk\sqrt{x^2+y^2+z^2}}}{\sqrt{x^2+y^2+z^2}}\right\} = \frac{1}{2\pi}K_0(\sqrt{p^2-k^2}\sqrt{y^2+z^2}). \tag{A7}$$

Thus, applying the shift and differential properties of the Fourier transformation to the image of Hertz's potential (A7) we get the following transformation rule:

$$\mathbf{L}_x\left\{\frac{1}{4\pi}\left(k^2+\frac{\partial^2}{\partial x^2}\right)\frac{e^{-jk\sqrt{x^2+y^2+z^2}}}{\sqrt{x^2+y^2+z^2}}\right\}$$
$$= \frac{1}{2\pi}(k^2-p^2)K_0(\sqrt{p^2-k^2}\sqrt{y^2+z^2}). \tag{A8}$$

Using Poisson's summation formulas (A6) together with (A8) we obtain the term C_2 in the form

$$C_2 = -\sum_{n\neq 0}\sum_{m=-\infty}^{+\infty}\frac{p_m^2}{2\pi a}K_0(p_m|bn|)e^{-jq_y bn}. \tag{A9}$$

If the arguments of McDonald's functions in Eq. (A9) have nonzero real part then the series with index n have very good convergence, but if these are imaginary then McDonald's functions transform to Hankel's functions and the mentioned series become slowly convergent. Therefore we separate the part of (A9) that has good convergence:

$$C_2' = -\sum_{n=1}^{+\infty} \sum_{\mathrm{Re}(p_m)\neq 0} \frac{p_m^2}{\pi a} K_0(p_m bn)\cos(q_y bn). \quad \text{(A10)}$$

The residual part of Eq. (A9) ($C_2' = C_2' + C_2''$),

$$C_2'' = -\sum_{n\neq 0} \sum_{\mathrm{Re}(p_m)=0} \frac{p_m^2}{2\pi a} K_0(p_m|bn|) e^{-jq_y bn}, \quad \text{(A11)}$$

which has slow convergence, should be calculated with the help of a special method. Note that there is only a finite number of indices m such that $\mathrm{Re}(p_m)=0$. This means that in Eq. (A11) the summation over the index m includes only a finite number of terms. For example, at the low frequency limit, when the period a is large compared with the wavelength in the host medium, the equation $\mathrm{Re}(p_m)=0$ has only one solution $m=0$ if $q_x<k$.

We will calculate the sum of the series (A11) as the limit with z tending to zero:

$$C_2'' = \lim_{z\to 0} \sum_{n\neq 0} \sum_{\mathrm{Re}(p_m)=0} \frac{-p_m^2}{2\pi a} K_0(p_m\sqrt{(bn)^2+z^2}) e^{-jq_y bn}. \quad \text{(A12)}$$

Introducing the auxiliary parameter z makes it possible to complement the series (A12) by the zeroth terms and then to use the Poisson summation formula over the index n [see Eq. (A3) for the necessary Fourier transform]. The result is as follows:

$$C_2'' = \lim_{z\to 0} \sum_{\mathrm{Re}(p_m)=0} \frac{-p_m^2}{2ab}\left(\sum_{n=-\infty}^{+\infty} \frac{e^{-j|z|k_z^{(mn)}}}{jk_z^{(mn)}} - \frac{b}{\pi} K_0(p_m|z|) \right). \quad \text{(A13)}$$

The term $K_0(p_m|z|)$ in Eq. (A13) plays the role of the zero term, which is subtracted from the complete series (already transformed using the Poisson summation formula) in order to get the series (A12) without the zero term. This term contains a singularity if z tends to zero. This singularity disappears in Eq. (A13) during subtraction from the complete series which experiences the same singularity. In order to cancel out these singularities analytically we apply the method of the dominant series; namely, we split the series from (A13) into dominant and correction parts:

$$\sum_{n=-\infty}^{+\infty} \frac{e^{-j|z|k_z^{(mn)}}}{jk_z^{(mn)}} = \sum_{n\neq 0} \left[\frac{e^{-j|z|k_z^{(mn)}}}{jk_z^{(mn)}} - b\frac{e^{-2\pi|z||n|/b}}{2\pi|n|} \right] + 2b\sum_{n=1}^{+\infty} \frac{e^{-2\pi|z|n/b}}{2\pi n} + \frac{e^{-j|z|k_z^{(m0)}}}{jk_z^{(m0)}}.$$

The dominant series can be evaluated using the tabulated formula (see [31], Appendix)

$$\sum_{n=1}^{+\infty} \frac{e^{-n\alpha}}{n} = -\ln(1-e^{-\alpha}). \quad \text{(A14)}$$

The whole singularity is included in the dominant series. The correction series have no singularity when z tends to zero. Using this fact the formula (A13) can be rewritten as

$$C_2'' = \sum_{\mathrm{Re}(p_m)=0} \frac{-p_m^2}{2ab}\left(\frac{1}{jk_z^{(m0)}} + \sum_{n\neq 0}\left[\frac{1}{jk_z^{(mn)}} - \frac{b}{2\pi|n|} \right] - \frac{b}{\pi}\lim_{z\to 0}[\log(1-e^{-2\pi|z|/b}) + K_0(p_m|z|)] \right). \quad \text{(A15)}$$

The logarithmic singularity occurring here is compensated by that arising from the term with the McDonald function. The small-argument expression for the McDonald function reads

$$K_0(\alpha) \to -[\gamma + \ln(\alpha/2)],$$

where $\gamma=0.577$ is Euler's constant.

Thus, the value of the limit in Eq. (A15) is as follows:

$$\lim_{z\to 0}[\cdot] = -\left(\ln\frac{b|p_m|}{4\pi} + \gamma + j\frac{\pi}{2} \right). \quad \text{(A16)}$$

The series in Eq. (A15) with index $n\in[-\infty,+\infty]$ except $n=0$ have convergence $1/n^2$. This convergence rate makes calculations not rapid enough. The convergence can be accelerated by extraction of the dominant series. In order to get the convergence $1/n^4$ it is enough to extract series of order $1/n^2$ and $1/n^3$:

$$\sum_{n=1}^{+\infty}\left[\frac{1}{jk_z^{(m,n)}} - \frac{b}{2\pi n} \right] = \sum_{n=1}^{+\infty}\left[\frac{1}{jk_z^{(m,n)}} - \frac{b}{2\pi n} + \frac{q_y b^2}{4\pi^2 n^2} - \frac{l_m b^3}{16\pi^3 n^3} \right] - \frac{q_y b^2}{24} + 1.202\frac{l_m b^3}{16\pi^3}, \quad \text{(A17)}$$

where $l_m = 2q_y^2 - p_m^2$, and we have taken into account that

$$\sum_{n=1}^{+\infty}\frac{1}{n^2} = \frac{\pi^2}{6}, \quad \sum_{n=1}^{+\infty}\frac{1}{n^3} = 1.202.$$

Collecting the terms corresponding to $+n$ and $-n$ together in Eq. (15) we obtain

$$\sum_{n\neq 0}\left[\frac{1}{jk_z^{(mn)}} - \frac{b}{2\pi|n|} \right] = \sum_{n=1}^{+\infty}\left[\frac{1}{jk_z^{(m,n)}} + \frac{1}{jk_z^{(m,-n)}} - \frac{b}{\pi n} \right] = \sum_{n=1}^{+\infty}\left[\frac{1}{jk_z^{(m,n)}} + \frac{1}{jk_z^{(m,-n)}} - \frac{b}{\pi n} - \frac{l_m b^3}{8\pi^3 n^3} \right] + 1.202\frac{l_m b^3}{8\pi^3}. \quad \text{(A18)}$$

The property $k_z^{(m,-n)}(q_x,q_y) = k_z^{(m,n)}(q_x,-q_y)$ makes the function

$$\frac{1}{jk_z^{(m,n)}} + \frac{1}{jk_z^{(m,-n)}} = \left[\frac{b/(2\pi|n|)}{\sqrt{(q_y b/(2\pi n)+1)^2 + p_m^2/(4\pi^2 n^2/b^2)}} + \frac{b/(2\pi|n|)}{\sqrt{(q_y b/(2\pi n)-1)^2 + p_m^2/(4\pi^2 n^2/b^2)}} \right]$$

even with respect to the variable $q_y b/(2\pi n)$. This means that, being expanded into a Taylor series, it will contain only even

power terms. Thus, the transformed series (A18) when expanded as a series of order $1/n$ will contain only odd-power terms. In Eq. (A18) we have already extracted the dominant series of order $1/n^3$. So we conclude that the series (A18) have convergence of order $1/n^5$, which is better than was estimated when we started to extract the dominant series in Eq. (A17).

Collecting the parts of the term C_2 given by Eqs. (A10), (A15), (A16), and (A18) we obtain the final formula for C_2 possessing convergence that is appropriate for rapid and effective numerical calculations:

$$C_2 = -\sum_{n=1}^{+\infty} \sum_{\mathrm{Re}(p_m)\neq 0} \frac{p_m^2}{\pi a} K_0(p_m bn)\cos(q_y bn) - \sum_{\mathrm{Re}(p_m)=0} \frac{p_m^2}{2ab}\left[\frac{1}{jk_z^{(m0)}} + \sum_{n=1}^{+\infty}\left(\frac{1}{jk_z^{(m,n)}} + \frac{1}{jk_z^{(m,-n)}} - \frac{b}{\pi n} - \frac{l_m b^3}{8\pi^3 n^3}\right) + 1.202\frac{l_m b^3}{8\pi^3} + \frac{b}{\pi}\left(\ln\frac{b|p_m|}{4\pi} + \gamma\right) + j\frac{b}{2}\right]. \tag{A19}$$

3. Contribution of the line located at x axis

The term C_3 has the form of the series [5,53]

$$C_3 = \frac{1}{2\pi a^3}\sum_{m\neq 0}\left(\frac{1}{|m|^3} + \frac{jka}{m^2}\right)e^{-j(k|am|+q_x am)}. \tag{A20}$$

These series have convergence that is not enough for effective direct numerical calculations. We will use the convergence acceleration technique presented in [52] in order to evaluate these series. The dominant series can be extracted in the following way:

$$\sum_{m=1}^{+\infty}\left(\frac{1}{m^3} + \frac{jka}{m^2}\right)e^{-jsm} = \sum_{m=1}^{+\infty}\left(\frac{1}{m^3} + \frac{jka}{m^2} - \frac{jka}{m(m+1)} - \frac{jka+1}{m(m+1)(m+2)}\right)e^{-jsm} + jka\sum_{m=1}^{+\infty}\frac{e^{-jsm}}{m(m+1)} + (jka+1)\sum_{m=1}^{+\infty}\frac{e^{-jsm}}{m(m+1)(m+2)}. \tag{A21}$$

The first series in the right-hand side of Eq. (A21) (that containing the expression in parentheses) can be simplified to

$$\sum_{m=1}^{+\infty}\frac{(2jka+3)m+2}{m^3(m+1)(m+2)}e^{-jsm}.$$

These series have convergence $1/m^4$ which is convenient for rapid calculations. The other series in the right-hand side of Eq. (A21) can be evaluated in the closed form using the formula (A14):

$$\sum_{m=1}^{+\infty}\frac{e^{-jsm}}{m(m+1)} = \sum_{m=1}^{+\infty}\frac{e^{-jsm}}{m} - \sum_{m=1}^{+\infty}\frac{e^{-jsm}}{m+1} = -(1-e^{js})\ln(1-e^{-js}) + 1,$$

$$\sum_{m=1}^{+\infty}\frac{e^{-jsm}}{m(m+1)(m+2)} = \frac{1}{2}\left[\sum_{m=1}^{+\infty}\frac{e^{-jsm}}{m(m+1)} - \sum_{m=1}^{+\infty}\frac{e^{-jsm}}{(m+1)(m+2)}\right] = -\frac{1}{2}\left[(1-e^{js})^2\ln(1-e^{-js}) + e^{js} - \frac{1}{2}\right].$$

After these manipulations the formula (A21) transforms as follows:

$$C_3 = \frac{1}{4\pi a^3}\left[4\sum_{m=1}^{+\infty}\frac{(2jka+3)m+2}{m^3(m+1)(m+2)}e^{-jkam}\cos(q_x am) - (jka+1)[t_+^2\ln t^+ + t_-^2\ln t^- + 2e^{jka}\cos(q_x a)] - 2jka(t_+\ln t^+ + t_-\ln t^-) + (7jka+3)\right], \tag{A22}$$

where

$$t^+ = 1 - e^{-j(k+q_x)a}, \quad t^- = 1 - e^{-j(k-q_x)a},$$

$$t_+ = 1 - e^{j(k+q_x)a}, \quad t_- = 1 - e^{j(k-q_x)a}.$$

The expression (A22) looks more cumbersome as compared to the initial formula (A20), but it is much more convenient for rapid calculations. The estimations show that in order to get accuracy of 0.01% one needs to take more than 200 terms in expression (A20) and only ten terms in (A22).

4. Energy conservation

In this subsection we evaluate the imaginary part of C and consider the problem of the energy balance in a 1D array (chain) of dipoles, in a 2D array (grid), and in a 3D array (lattice).

Let us return to formula (A20) and find the imaginary part of the interaction constant of the dipole chain:

$$\mathrm{Im}(C_3) = \frac{1}{\pi a^3}\sum_{m=1}^{\infty}\cos q_x am\left(\frac{\sin kam}{m^3} - ka\frac{\cos kam}{m^2}\right). \tag{A23}$$

To calculate these series we used the auxiliary formulas

$$\sum_{m=1}^{+\infty}\frac{\cos sm}{m^2} = \frac{(\pi - s')^2}{4} - \frac{\pi^2}{12}, \tag{A24}$$

$$\sum_{m=1}^{+\infty}\frac{\sin sm}{m^3} = \frac{s'^3 - 3\pi s'^2 + 2\pi^2 s'}{12}. \tag{A25}$$

These formulas can be easily obtained from the relation (A14) rewritten for the case $\alpha = js$,

$$\sum_{m=1}^{+\infty} \frac{e^{-jsm}}{m} = -\ln(1-e^{-js}) = -\left(\ln\left|2\sin\frac{s}{2}\right| + j\frac{\pi - s'}{2}\right), \tag{A26}$$

where $s' = 2\pi\{s/(2\pi)\}$ and we use the notation $\{x\}$ for the fractional part of the variable x. To derive Eqs. (A24) and (A25) one should integrate Eq. (A26) over the parameter s.

Note that the real part of C_3 contains the series

$$\sum_{m=1}^{+\infty} \frac{\sin sm}{m^2} \quad \text{and} \quad \sum_{m=1}^{+\infty} \frac{\cos sm}{m^3}, \tag{A27}$$

which can be expressed in terms of second and third order repeating integrals of the tangent function. These integrals cannot be evaluated in elementary functions, but they are suitable for numerical calculations. We prefer to use the acceleration technique leading to the result (A22) for evaluation of C_3, rather than using numerical integration. Some other recommendations for calculation of the series (A27) can be found in [31] together with their expansions into Taylor series.

After substitution of Eqs. (A24) and (A25) into Eq. (A23) and some algebra the following compact form for $\mathrm{Im}(C_3)$ can be obtained:

$$\mathrm{Im}(C_3) = \frac{k^3}{6\pi} + \frac{1}{4a}\sum_{|k_x^{(m)}|<k} p_m^2. \tag{A28}$$

It is easy to obtain the imaginary parts of C_2 and C_1. The imaginary part of formula (A19) reads

$$\mathrm{Im}(C_2) = \sum_{\mathrm{Im}(k_z^{(mn)})=0} \frac{p_m^2}{2abk_z^{(mn)}} - \sum_{|k_x^{(m)}|<k} \frac{p_m^2}{4a}. \tag{A29}$$

The imaginary part of formula (A5) reads

$$\mathrm{Im}(C_1) = -\sum_{\mathrm{Im}(k_z^{(mn)})=0} \frac{p_m^2}{2abk_z^{(mn)}}. \tag{A30}$$

Collecting together Eqs. (A28)–(A30) we obtain that

$$\mathrm{Im}(C) = \frac{k^3}{6\pi}. \tag{A31}$$

This relation makes the dispersion equation (13) real valued for the case of propagating modes.

Now, let us discuss the energy balance in the chain using the result (A28). If the dipoles are arranged in a periodical linear array $x=am$ phased by a wave vector with x component q_x (as in [53]) then the structure radiates cylindrical waves. The number of these waves depends on the relation between the wavelength, chain period, and phase constant q_x. In the regime of the guided mode $q_x > k$ this number is zero since $|k_x^{(m)}| > k$ for all m. Using the Sipe-Kranendonk condition (2) for the imaginary part of the polarizability's inverse value one can obtain a purely real valued dispersion equation for the guided mode in the chain [5,53]:

$$\mu_0\alpha^{-1}(\omega) - C_3(\omega, q_x, a) = 0.$$

However, the arrangement of the dipoles into an array changes the radiation losses of the individual scatterers. The effective polarizability of the scatterer in the linear array becomes as follows:

$$\alpha_1 = (\alpha^{-1} - \mu_0^{-1}C_3)^{-1}.$$

The Sipe-Kranendonk condition in the general case of radiated waves should be replaced by

$$\mathrm{Im}(\alpha_1^{-1}) = \sum_{|k_x^{(m)}|<k} \frac{-p_m^2}{4a\mu_0}. \tag{A32}$$

The expression (A32) follows from the formulas (2) and (A28). This relation expresses the balance between the radiation losses of the individual scatterer of the chain and the contribution of the chain unit cell into the radiated waves ($|k_x^{(m)}| < k$).

Now, consider a 2D grid of dipoles located at the nodes with coordinates $x=am$ and $y=bn$ and phased by real q_x and q_y, respectively. The effective polarizability of a scatterer in this planar grid is

$$\alpha_2 = (\alpha_1^{-1} - \mu_0^{-1}C_2)^{-1} = [\alpha^{-1} - \mu_0^{-1}(C_2 + C_3)]^{-1}. \tag{A33}$$

The formulas (A33) and (A29) allow us to formulate an analog of the Sipe-Kranendonk condition for the planar grid:

$$\mathrm{Im}(\alpha_2^{-1}) = \sum_{\mathrm{Im}(k_z^{(mn)})=0} \frac{-p_m^2}{2ab\mu_0 k_z^{(mn)}}. \tag{A34}$$

The terms $-p_m^2/(4a\mu_0)$ corresponding to the cylindrical waves in Eq. (A32) are canceled out by the respective terms from Eq. (A29) and replaced by the terms $p_m^2/(2ab\mu_0 k_z^{(mn)})$. The last ones correspond to the radiated plane waves [Floquet harmonics with indices (m,n) produced by the grid]. The condition $\mathrm{Im}(k_z^{(mn)})=0$ for the finite sum in Eq. (A34) is the radiation condition for these Floquet harmonics. Formula (A34) expresses the balance between the radiation losses of the dipole and the contribution of the grid unit cell to the radiation.

In the surface wave regime, when $\mathrm{Im}(k_z^{(mn)}) \neq 0$ for all m,n, using the Sipe-Kranendonk condition (2) one can obtain a real valued dispersion equation for the surface wave propagating along the grid:

$$\mu_0\alpha^{-1}(\omega) - \tilde{C}_2(\omega, q_x, q_y, a, b) = 0,$$

where

$$\tilde{C}_2(\omega, q_x, q_y, a, b) = C_2(\omega, q_x, q_y, a, b) + C_3(\omega, q_x, a).$$

Finally, let us consider a 3D lattice with nodes $x=am$, $y=bn$, and $z=cl$ phased by real q_x, q_y, and q_z respectively. The effective polarizability of the scatterer in this lattice is

$$\alpha_3 = (\alpha_2^{-1} - C_1)^{-1} = (\alpha^{-1} - C)^{-1}. \quad \text{(A35)}$$

From Eqs. (A30), (A35), and (A34) we easily obtain

$$\mathrm{Im}(\alpha_3^{-1}) = 0. \quad \text{(A36)}$$

The terms $p_m^2/(2ab\mu_0 k_z^{(mn)})$ in Eq. (A34) are canceled by the respective terms of Eq. (A30). Physically, this means that radiation losses of the scatterer in this lattice are zero. The lattice does not radiate power because it fills the whole space and the radiation losses of the single scatterer are compensated by the electromagnetic interaction in the lattice (as well as in the waveguide regimes of the chain and of the grid).

5. Final formula

Collecting together the results (A5), (A19), and (A20) we obtain the final expression for the dynamic interaction constant:

$$\begin{aligned} C(k,\mathbf{q},a,b,c) = \frac{1}{4\pi a^3}\Bigg[& 4\sum_{m=1}^{+\infty} \frac{(2jka+3)m+2}{m^3(m+1)(m+2)} e^{-jkam}\cos(q_x am) - (jka+1)[t_+^2 \ln t^+ + t_-^2 \ln t^- + 2e^{jka}\cos(q_x a)] \\ & - 2jka(t_+ \ln t^+ + t_- \ln t^-) + (7jka+3)\Bigg] - \sum_{n=1}^{+\infty} \sum_{\mathrm{Re}(p_m)\neq 0} \frac{p_m^2}{\pi a} K_0(p_m bn)\cos(q_y bn) \\ & + \sum_{m=-\infty}^{+\infty}\sum_{n=-\infty}^{+\infty} \frac{p_m^2}{2jabk_z^{(mn)}} \frac{e^{-jk_z^{(mn)}c} - \cos q_z c}{\cos k_z^{(mn)} c - \cos q_z c} - \sum_{\mathrm{Re}(p_m)=0} \frac{p_m^2}{2ab}\left(\frac{1}{jk_z^{(m0)}} + \sum_{n=1}^{+\infty}\left[\frac{1}{jk_z^{(m,n)}} + \frac{1}{jk_z^{(m,-n)}} - \frac{b}{\pi n} - \frac{l_m b^3}{8\pi^3 n^3}\right]\right. \\ & \left. + 1.202\frac{l_m b^3}{8\pi^3} + \frac{b}{\pi}\left[\ln\frac{b|p_m|}{4\pi} + \gamma\right] + j\frac{b}{2}\right), \end{aligned} \quad \text{(A37)}$$

where we use the following notations (introduced above and collected here):

$$k_x^{(m)} = q_x + \frac{2\pi m}{a}, \quad k_y^{(n)} = q_y + \frac{2\pi n}{b},$$

$$p_m = \sqrt{(k_x^{(m)})^2 - k^2}, \quad l_m = 2q_y^2 - p_m^2,$$

$$k_z^{(mn)} = -j\sqrt{(k_x^{(m)})^2 + (k_y^{(n)})^2 - k^2}.$$

$$t^+ = 1 - e^{-j(k+q_x)a}, \quad t^- = 1 - e^{-j(k-q_x)a},$$

$$t_+ = 1 - e^{j(k+q_x)a}, \quad t_- = 1 - e^{j(k-q_x)a}.$$

The calculations using Eq. (A37) can be restricted to the real part only, because its imaginary part is predefined by Eq. (A31). The series in Eq. (A37) have excellent convergence which ensures very rapid numerical calculations.

6. Low frequency limit case

It is useful to consider the low frequency limit (when k, q_x, q_y, and q_z are small as compared with $1/a$, $1/b$, and $1/c$) and show that the result for C transits to the known one for this case. Following the definition (A20) for term C_3 we conclude that

$$C_3 = \frac{1}{\pi a^3}\sum_{m=1}^{+\infty}\frac{1}{m^3} = \frac{1.202}{\pi a^3}.$$

The expression (A19) for C_2 reduces to

$$C_2 = -\frac{8\pi}{a^3}\sum_{m=1}^{+\infty}\sum_{n=1}^{+\infty} m^2 K_0\left(\frac{2\pi m}{a} bn\right).$$

Note that both C_3 and C_2 turn out to be independent of k and $\mathbf{q}$. The formula (A5) for C_1 splits into two terms: the first one, which depends on k and $\mathbf{q}$ (where we have expanded trigonometric functions into Taylor series), and some additional constant,

$$C_1 = -\frac{1}{abc}\frac{k^2 - q_x^2}{k^2 - q_x^2 - q_y^2 - q_z^2} - \frac{4\pi}{a^2 b}\sum_{m=1}^{+\infty}\frac{m}{e^{2\pi mc/a} - 1} - \frac{8\pi}{a^3}\sum_{m=1}^{+\infty}\sum_{n=1}^{+\infty}\frac{m^2/\sqrt{(bm/a)^2 + n^2}}{e^{2\pi\sqrt{(bm/a)^2+n^2}c/b} - 1}.$$

Finally, we get

$$C = -\frac{1}{abc}\frac{k^2 - q_x^2}{k^2 - q_x^2 - q_y^2 - q_z^2} + C_s(a,b,c), \quad \text{(A38)}$$

where $C_s(a,b,c)$ is the static interaction constant (7), and obtain the alternative representation for $C_s(a,b,c)$

$$C_s(a,b,c) = \frac{1.202}{\pi a^3} - \frac{8\pi}{a^3}\left[\sum_{m=1}^{+\infty}\sum_{n=1}^{+\infty}\frac{m^2/\sqrt{(bm/a)^2+n^2}}{e^{2\pi\sqrt{(bm/a)^2+n^2}c/b} - 1} + \frac{a}{2b}\sum_{m=1}^{+\infty}\frac{m}{e^{2\pi mc/a} - 1} + \sum_{m=1}^{+\infty}\sum_{n=1}^{+\infty} m^2 K_0\left(\frac{2\pi m}{a} bn\right)\right]. \quad \text{(A39)}$$

The static interaction constant expressed as (A39) is equiva-

lent to (7). The expression (A39) can be obtained from Eq. (7) by applying the Poisson summation formula over the index n and then by direct summation over the index l (in the same manner as was done above during evaluation of the term C_1). Both formulas (A39) and (7) are extremely effective for rapid numerical calculations due to excellent convergence of the series. The difference between (7) and (A39) is that (7) contains triple series in contrast to (A39) which comprises only double ones. It is noteworthy that the convergence of the series in (7) is higher than in (A39).

The formula (A38) when substituted into Eq. (13) reduces the dispersion equation for an electromagnetic crystal to the known dispersion equation of a continuous uniaxial magnetic material (8) with magnetic permittivity of the form (6). This fact is an important verification of the introduced dispersion theory.

[1] J. Sipe and J. V. Kranendonk, Phys. Rev. A **9**, 1806 (1974).
[2] A. Serdyukov, I. Semchenko, S. Tretyakov, and A. Sihvola, *Electromagnetics of Bi-Anisotropic Materials: Theory and Applications* (Gordon and Breach Science Publishers, Amsterdam, 2001).
[3] I. Lindell, A. Sihvola, S. Tretyakov, and A. Viitanen, *Electromagnetic Waves and Bi-Isotropic Media* (Artech House Publishers, Boston, MA, 1994).
[4] S. Ponti, J. Reyes, and C. Oldano, J. Phys.: Condens. Matter **14**, 10173 (2002).
[5] W. H. Weber and G. W. Ford, Phys. Rev. B **70**, 125429 (2004).
[6] A. Alu, A. Salandrino, and N. Engheta, e-print cond-mat/0412263.
[7] V. Veselago, Sov. Phys. Usp. **10**, 509 (1968).
[8] J. Pendry, Phys. Rev. Lett. **85**, 3966 (2000).
[9] D. R. Smith, W. J. Padilla, D. C. Vier, S. C. Nemat-Nasser, and S. Schultz, Phys. Rev. Lett. **84**, 4184 (2000).
[10] R. A. Shelby, D. R. Smith, and S. Schultz, Science **292**, 77 (2001).
[11] A. A. Houck, J. B. Brock, and I. L. Chuang, Phys. Rev. Lett. **90**, 137401 (2003).
[12] J. Brown, Prog. Dielectr. **2**, 195 (1960).
[13] W. Rotman, IRE Trans. Antennas Propag. **10**, 82 (1962).
[14] J. B. Pendry, A. J. Holden, W. J. Stewart, and I. Youngs, Phys. Rev. Lett. **76**, 4773 (1996).
[15] J. Pendry, A. Holden, D. Robbins, and W. Stewart, IEEE Trans. Microwave Theory Tech. **47**, 2075 (1999).
[16] P. A. Belov, R. Marques, S. I. Maslovski, I. S. Nefedov, M. Silveirinha, C. R. Simovski, and S. A. Tretyakov, Phys. Rev. B **67**, 113103 (2003).
[17] S. Tretyakov, S. Maslovski, and P. A. Belov, IEEE Trans. Antennas Propag. **51**, 2652 (2003).
[18] R. Ziolkowski, IEEE Trans. Antennas Propag. **51**, 1516 (2003).
[19] C. Simovski and S. He, Phys. Lett. A **311**, 254 (2003).
[20] E. Verney, B. Sauviac, and C. Simovski, Phys. Lett. A **331**, 244 (2004).
[21] D. R. Smith and D. Schurig, Phys. Rev. Lett. **90**, 077405 (2003).
[22] D. R. Smith, P. Kolinko, and D. Schurig, J. Opt. Soc. Am. B **21**, 1032 (2004).
[23] D. R. Smith, D. Schurig, J. J. Mock, P. Kolinko, and P. Rye, Appl. Phys. Lett. **84**, 2244 (2004).
[24] I. Lindell, S. Tretyakov, K. Nikoskinen, and S. Ilvonen, Microwave Opt. Technol. Lett. **31**, 129 (2001).
[25] P. Belov, Microwave Opt. Technol. Lett. **37**, 259 (2003).
[26] P. A. Belov, S. A. Tretyakov, and A. J. Viitanen, Phys. Rev. E **66**, 016608 (2002).
[27] R. Marques, F. Medina, and R. Rafii-El-Idrissi, Phys. Rev. B **65**, 144440 (2002).
[28] B. Sauviac, C. Simovski, and S. Tretyakov, Electromagnetics **24**, 317 (2004).
[29] C. Simovski, P. A. Belov, and S. He, IEEE Trans. Antennas Propag. **51**, 2582 (2003).
[30] P. Belov, S. Maslovski, C. Simovski, and S. Tretyakov, Tech. Phys. Lett. **29**, 36 (2003).
[31] R. Collin, *Field Theory of Guided Waves* (IEEE Press, Piscataway, NJ, 1990).
[32] B. Nijboer and F. de Wette, Physica (Amsterdam) **24**, 422 (1958).
[33] F. de Wette and G. Schacher, Phys. Rev. **137**, A78 (1965).
[34] M. Kharadly and W. Jackson, Proc. IRE **100**, 199 (1962).
[35] P. P. Ewald, Ann. Phys. **64**, 253287 (1921).
[36] M. G. Silveirinha and C. A. Fernandes, IEEE Trans. Microwave Theory Tech. **53**, 347 (2005).
[37] M. G. Silveirinha and C. A. Fernandes, IEEE Trans. Microwave Theory Tech. **52**, 889 (2004).
[38] N. A. Nicorovici, R. C. McPhedran, and Bao Ke-Da, Phys. Rev. E **51**, 690 (1995).
[39] A. Borji and S. Safavi-Naeni, IEEE Trans. Microwave Theory Tech. **52**, 1724 (2004).
[40] A. Kustepeli and A. Martin, IEEE Microw. Guid. Wave Lett. **10**, 168 (2000).
[41] M. Notomi, Phys. Rev. B **62**, 10696 (2000).
[42] C. Luo, S. G. Johnson, J. D. Joannopoulos, and J. B. Pendry, Phys. Rev. B **65**, 201104(R) (2002).
[43] P. Belov, C. Simovski, and P. Ikonen, Phys. Rev. B **71**, 193105 (2005).
[44] D. N. Chigrin, S. Enoch, C. M. S. Torres, and G. Tayeb, Opt. Express **11**, 1203 (2003).
[45] H.-T. Chien, H.-T. Tang, C.-H. Kuo, C.-C. Chen, and Z. Ye, Phys. Rev. B **70**, 113101 (2004).
[46] Z.-Y. Li and L.-L. Lin, Phys. Rev. B **68**, 245110 (2003).
[47] C.-H. Kuo and Z. Ye, Phys. Rev. E **70**, 056608 (2004).
[48] C. Luo, S. G. Johnson, J. D. Joannopoulos, and J. B. Pendry, Phys. Rev. B **68**, 045115 (2003).
[49] K. Aydin, K. Guven, N. Katsarakis, C. M. Soukoulis, and E. Ozbay, Opt. Express **12**, 5896 (2004).
[50] E. Smith, J. Phys. A **13**, L107 (1980).
[51] P. Belov, S. Tretyakov, and A. Viitanen, J. Electromagn. Waves Appl. **16**, 1153 (2002).
[52] L. Kantorovich and V. Krylov, *Approximate Methods of Higher Analysis* (Interscience Publishishers, New York, 1958).
[53] S. Tretyakov and A. Viitanen, Electr. Eng. **82**, 353 (2000).